ACES Asian Chemical Editorial Society

doi.org/10.1002/ajoc.202500546

ASIAN JOURNAL OF ORGANIC CHEMISTRY
Research Article

www.asianjoc.org

Electron Donating Group Effect on C—C Bond Scission Ability of Indanedione Dimers in Their Solution and Solid State

Yukina Yamamoto,[a] Yumi Yakiyama,*[a, b, c] Tomohiko Nishiuchi,[b, d] Takashi Kubo,[b, d] and Hidehiro Sakurai[a, b]

In memory of Professor Masahiko Iyoda

Light, heat and mechanical stress-responsive molecules are of great interest in the field of modern materials chemistry. In this work, indanedione dimers **1**–**3** introduced with an electron-donating thiophene group were designed with the expectation of easy cleavage of the central C—C single bond by the captodative effect. Our synthetic approach led to the successful preparation of dimethylthiophenyl and methylbenzothiophenyl derivatives **1** and **2**, while benzothiophenyl compound **3** was not formed; instead, the bridged product **3′** was obtained. The sequential UV–vis absorption and ESR measurements of **1** and **2** in the solution state confirmed the effectiveness of the presence of an electron-donating group, which stabilized the radical form to realize a relatively low bond cleavage temperature. Meanwhile, it was also clarified that the bond scission event was strongly affected by the packing structure; much harder in the tightly packed crystalline **1** than its solution state, while almost the same as the solution state in the glassy solid of **2**, in which the intermolecular interaction should be much weaker and each molecule could move as easily as in the solution state. Further investigation of **3′** revealed the loss of bond scission ability by bridging.

1. Introduction

Stimuli-responsive materials, which change their physical properties in response to external stimuli (light, heat, mechanical stress, etc.) are widely studied for potential applications such as sensors and actuators.[1–7] Common mechanisms that trigger such property changes include structural isomerization, inter- or intramolecular charge transfer, and the dynamic covalent bond.[8–10] Among them, systems that undergo homolytic bond cleavage to generate radicals often exhibit distinct color changes.[10] For example, hexaarylbimidazoles are well known to exhibit bond cleavage upon UV irradiation,[11] and the corresponding radical stability changes with substituents, resulting in changes in color and lifetime. Benzofuranone dimers are also other good examples, and the polymers incorporating them in the main chain change the color in the stressed area and provide self-healing ability by promoting reversible bond cleavage.[12]

Indanedione dimers are known to undergo central C—C bond scission by heat, light, or shear stress.[13–18] In particular, a derivative having an electron-donating dimethylaminophenyl (Me_2NPh) group generates radicals associated with bond cleavage at 60 °C in benzene solution,[13] and its bond-scission behavior has been investigated in detail. We recently reported the γ-pyridyl-substituted derivative **4PID**, which exhibits unique structural flexibility, allowing for crystallinity-retained structure transformation between tightly packed- and solvent-incorporated structures via the uptake and the release of solvent molecules (Figure 1).[19] This result indicates that indanedione dimers possess the potential to construct a variety of soft assembled structures.[20] If such flexibility could be coupled with the intrinsic C—C bond scission ability of indanedione dimers, it may lead to a new class of crystalline materials with functions linked to radical generation, such as color change, electron conduction, adhesion, etc.[21,22] In this context, we revisited the previous report about the C—C bond scission properties of various indanedione dimers bearing electron-donating groups such as Me_2NPh, tBu, iPr_3Ph, and mesityl in the solution state,[13] which demonstrated enhanced bond scission ability. These results suggest the involvement of a radical stabilization

[a] Y. Yamamoto, Dr. Y. Yakiyama, Prof. Dr. H. Sakurai
Division of Applied Chemistry, Graduate School of Engineering, The University of Osaka, 2-1 Yamadaoka, Suita, Osaka 565–0871, Japan
E-mail: yakiyama@chem.eng.osaka-u.ac.jp

[b] Dr. Y. Yakiyama, Dr. T. Nishiuchi, Prof. Dr. T. Kubo, Prof. Dr. H. Sakurai
Innovative Catalysis Science Division, Institute for Open and Transdisciplinary Research Initiatives (ICS-OTRI), The University of Osaka, 2-1 Yamadaoka, Suita, Osaka 565–0871, Japan

[c] Dr. Y. Yakiyama
PRESTO, Japan Science and Technology Agency (JST), Kawaguchi, Saitama 332-0012, Japan

[d] Dr. T. Nishiuchi, Prof. Dr. T. Kubo
Department of Chemistry, Graduate School of Science, The University of Osaka, 1-1 Machikaneyama-cho, Toyonaka, Osaka 560–0043, Japan

Supporting information for this article is available on the WWW under https://doi.org/10.1002/ajoc.202500546

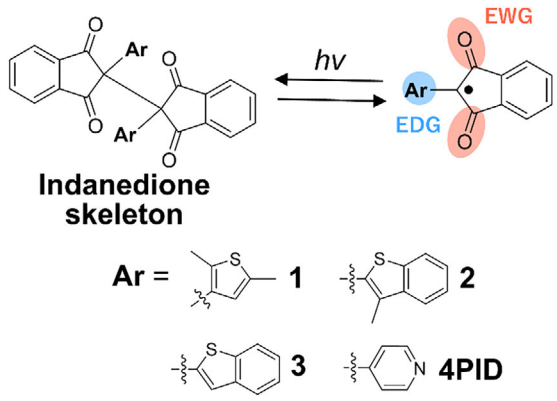

Figure 1. Molecular structures of the targeted **1**–**3** and **4PID**, as well as the concept of this work.

effect by the so-called "captodative (push-pull) effect",[23,24] where the radical center is flanked by both electron-donating and accepting groups. Based on this knowledge, we newly designed indanedione dimers incorporating electron-donating thiophene units **1**–**3** (Figure 1). Especially, we expected that **2** and **3** would exhibit lower C—C bond scission temperature due to the additional less-dense packing effect attributed to the fused ring to the thiophene skeleton. During the study, we unexpectedly obtained a bridged compound **3'** instead of **3** and investigated their solution- and solid-state C—C bond scission properties in comparison with the case of **4PID**. Our results clearly revealed that the introduction of thiophene group effectively affected electronically to reduce the bond scission temperature in the solution state, while in the solid state, intermolecular interaction strength significantly affected the bond scission property.

2. Results and Discussion

2.1. Initial Assessment of Bond Dissociation Energy (BDE) by Quantum Chemical Calculation

Before proceeding to the synthesis, we first evaluated the ease of central C—C bond cleavage by estimating the bond dissociation energy (BDE), defined as the energy gap between the dimer and the corresponding two monomers, via density functional theory (DFT) calculation at the B3LYP-D3/6-311G(d,p) level of theory (Figure 2).

The BDE for the previously reported Me_2NPh derivative was calculated to be 22.90 kcal/mol. Compounds **1**, **2**, and **3** showed 32.99, 26.39, and 26.39 kcal/mol, respectively. All of them are lower than that of **4PID** (41.54 kcal/mol). These results suggest that compounds **1**–**3** are expected to exhibit lower bond-scission temperatures compared with **4PID**.

2.2. Synthesis of Thiophene-Substituted Indanedione Dimers

The synthesis of the three new indanedione dimers was carried out as shown in Scheme 1. The corresponding aldehyde precursors were prepared according to the previously reported

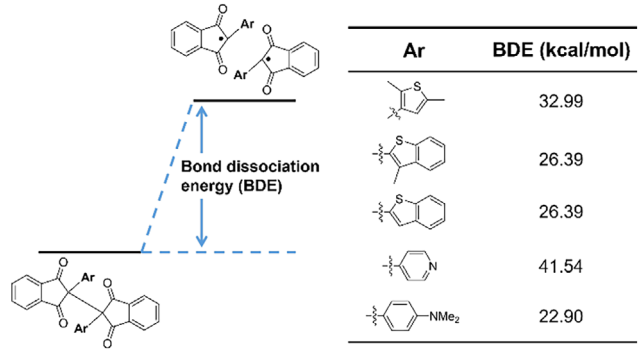

Figure 2. Schematic model of bond dissociation energy (BDE) and the summary of BDE for **1**–**3**, **4PID**, and Me_2NPh derivative.

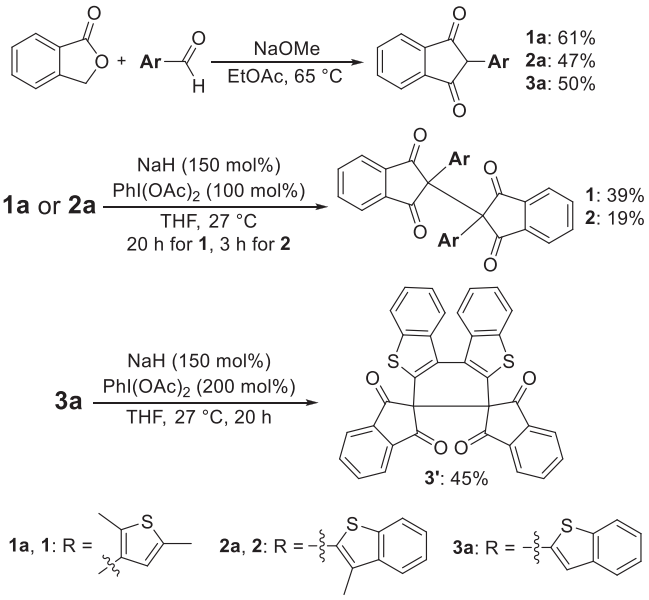

Scheme 1. Synthetic scheme of **1**–**3**. For the preparation of **1a**–**3a**, 400 mol% of NaOMe and 18 h reaction time were applied for **2a** and **3a**, while 300 mol% of NaOMe with 6 h of stirring for **1a**.

procedures.[25–27] These aldehydes were treated with phthalide under basic conditions using sodium methoxide in EtOAc to give the monomer products **1a**-**3a** in moderate yields.[28] For the subsequent dimerization via oxidative coupling, we initially employed $PhI(OAc)_2$ as the oxidant and sodium methoxide as the base, based on its prior success in the preparation of **4PID**. However, in the case of electron-donating ring-substituted monomers, a major byproduct, an α-methoxy substituted monomer, was observed. As a result, the yield of the desired dimer was limited to below 10%. When bulky potassium *t*-butoxide was instead used as a base, the yield of **1** was improved to 20%, although a side product containing a *t*-butoxy group was still formed. Finally, sodium hydride proved effective in suppressing side reactions involving nucleophilic substitution, enabling the successful preparation of desired indanedione dimers **1** and **2** in 39% and 19% yields, respectively. In contrast, the compound **3** was not obtained due to the C—C bond formation at the β-position of the thiophene ring, giving the

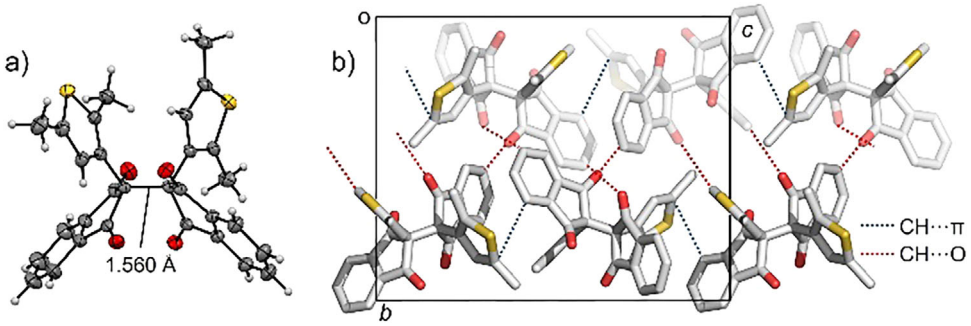

Figure 3. Crystal structure of **1**. a) Thermal ellipsoid plot at the 50% probability. b) *a*-axis projection of the crystal structure of **2**. C, grey; O, red; S, yellow. Hydrogen atoms were omitted for clarity.

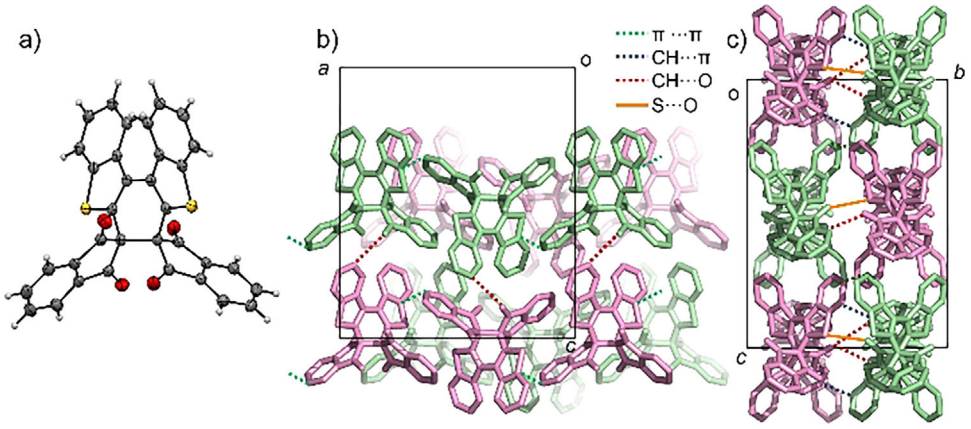

Figure 4. Crystal structure of **3′**. a) Thermal ellipsoid plot at the 50% probability. b) *b*-axis, and c) *a*-axis projections of the crystal structure of **3′**. For b) and c), Λ and Δ forms of the helices were represented with green and pink, respectively. C, grey; O, red; S, yellow. Hydrogen atoms were omitted for clarity.

bridged product **3′** in 45% yield. All products are characterized by ^{1}H and ^{13}C NMR, HRMS, and elemental analysis.

We next focused on obtaining single crystals of **1**, **2**, and **3′**. Single crystals of **1** were successfully obtained as yellow block crystals by the vapor diffusion method using dichloromethane and hexane. X-ray single crystal structure analysis revealed its tightly packed structure as shown in Figure 3. The central C—C bond did not show significant elongation to be 1.560 Å, which was comparable with the reported indanedione derivatives.[19,20] The packing structure was exclusively connected via weak intermolecular interaction, including CH···π interactions (3.725 Å) between the aromatic ring of indanedione and the thiophene skeleton and CH···O interaction between C═O group of the indanedione skeleton and the aromatic ring (3.109, 3.207 Å) or methyl group (3.304 Å) (Figure 3b). Also, single crystals of the bridged compound **3′** were obtained by slow evaporation of dichloromethane solution as deep orange crystals. Structural analysis revealed a helicene-like twisted structure, indicating the possibility of racemization (Figure 4). As expected, both right-handed Λ (green) and left-handed Δ (pink) helices were observed, forming a racemic mixture (Figure 4b). In the packing structure, there was 1D chain structure of the same helices along the *a*-axis via $\pi\cdots\pi$ interaction (3.386 Å) between the benzene rings, which were further connected along the *c*-axis by weak CH···O type interaction (3.291, 3.297 Å) between the indanedione C═O and benzothiophene moiety. Chains of the opposite helix along the *b*-axis were bound by CH···π interaction (3.733 Å) between benzothiophenes, CH···O interaction (3.386, 3.389 Å) between the indanedione C═O and benzothiophene moiety, and S···O contacts (3.209 Å) between the indanedione C═O and thiophene ring. The confirmation of the racemic mixture of **3′** prompted attempts to isolate the individual Λ and Δ enantiomers. However, chiral separation proved unsuccessful due to the low isomerization energy (<10 kcal/mol), as estimated by DFT calculations (Figure S1). Despite extensive efforts under various conditions, single crystals of **2** were not obtained. Instead, we confirmed the formation of a glass-like solid of **2** under vapor diffusion using CH_2Cl_2/hexane condition at −30 °C (Figure S2). Glass material formation is of great interest, especially in pharmaceutical chemistry[29] as well as optics.[30] In these fields, their amorphous nature realizes the high processability, and the property also affected the present system (vide infra).

2.3. Solution-State Properties of 1, 2, 3′, and 4PID

With the targeted materials in hand, we started to investigate the heat-induced C—C bond scission property of **1**, **2′**, and **3**. Initial assessments were conducted using solution-state UV–vis

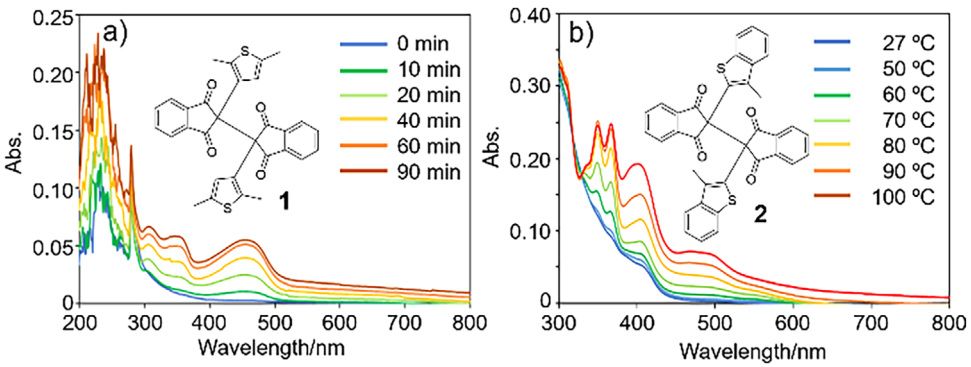

Figure 5. High-temperature UV–vis absorption measurement of **1** and **2**. a) Time dependency of UV absorption changes in **1** at 100 °C in toluene (1.0×10^{-5} M solution). b) Temperature dependency of UV–vis absorption spectra changes in **2** from 27 °C to 100 °C in toluene (1.0×10^{-5} M solution).

absorption and ESR spectroscopy with toluene as the solvent. Compound **1** exhibited no change upon heating to 100 °C, with no absorption observed at wavelengths longer than 400 nm (Figure 5). However, upon prolonged heating at 100 °C, a new peak gradually appeared in the visible region, accompanied by a broad absorption tail at the longer wavelength, both increasing in intensity over time. These results indicate the cleavage of the central C—C bond and the subsequent formation of monomer radicals. Time-dependent (TD)-DFT simulations of **1** well supported this interpretation (Figure S3). In compound **2**, a new broad absorption peak between 330 and 600 nm appeared upon heating to approximately 50 °C, with its intensity increasing with temperature. This behavior, similar to that of compound **1**, also points to the formation of thermally generated monomer radicals and was likewise well reproduced by TD-DFT calculations. In contrast, **4PID** exhibited no significant changes in UV–vis absorption measurement even at 100 °C, indicating that the introduction of the electron-donating thiophene unit in compounds **1** and **2** is responsible for the thermally induced the spectral changes (Figure S4a). Meanwhile, no clear change was observed in the UV–vis absorption spectra of **3'** even after 2 h of heating up at 100 °C, indicating that the intrinsic bond-scission property of the indanedione dimer skeleton was lost (Figure S4b).

Next, high-temperature electron spin resonance (ESR) measurements were performed to directly confirm the formation of monomer radical species using mesitylene as the solvent. In the case of compound **1**, a distinct signal ($g = 2.0073$) with hyperfine coupling was observed at 110 °C. The ESR signal pattern closely matched the simulated spectrum of the monomer radical **1**$^{\bullet}$ based on the spin density obtained from DFT calculation, though a slight deviation was confirmed, which was probably attributable to the dimethylthiophene ring rotation causing the fluctuation of the spin density distribution (Figure 6a, see Electronic Supporting Information). ^{1}H NMR spectra of the ESR sample after heating to 160 °C in mesitylene showed the monomer **1a** signal as a major component instead of the initial dimer **1**, indicating that reformation of the C—C bond did not occur in solution (Figure S5). On the other hand, a weak signal ($g = 2.0043$) originating from the radical species was already observed at room temperature in **2**, and its intensity increased with heating to 70 °C. Its splitting pattern of the signal with hyperfine coupling was also in good agreement with the simulated pattern of the corresponding radical **2**$^{\bullet}$, confirming the cleavage of the central C—C bond and generation of the corresponding radical species (Figure 6b, see Electronic Supporting Information). Upon further heating to 90 °C, the ESR signal profile began to change, and its intensity gradually diminished at temperatures up to 150 °C (Figure S6a). Notably, the original ESR pattern did not recover upon cooling, suggesting that irreversible radical reactions occurred, leading to the formation of new chemical species. This was also confirmed by the temperature-dependent ^{1}H NMR measurement in deuterated toluene, affording the corresponding monomer **2a** as a major product along with unidentified aromatic byproducts (Figure S6b). As in the case of UV measurement, the ESR signal of **4PID** never be observed below 100 °C (Figure S7a), indicating that the presence of the electron-donating thiophene unit plays a crucial role in facilitating C—C bond cleavage via the captodative effect, as predicted by DFT calculations. In contrast, compound **3'** displayed no detectable ESR signal even after heating to 150 °C (Figure S7b), supporting the conclusion from UV–vis absorption measurement that the bridged structure of **3'** inherently lacks bond-scission capability.

2.4. Solid-State Properties of 1, 2, and 4PID

As we confirmed the electric effect of electron-donating thiophene ring, next the solid-state packing effect was investigated, finding how low crystallinity of **2** affected its solid-state properties. The investigation was initiated by the diffuse reflectance spectra analysis (Figure 7). Powder samples of each compound were heated using a small electric furnace, and diffuse reflection measurements were performed before and after the heating. In powder crystalline **1**, it was found that an absorption peak between 400 and 600 nm appeared after heating to 180 °C for 2 h, which was not confirmed before heating (Figure 7a). Compound **2** also showed a peak with slightly broadened absorption at longer wavelengths after heating to about 110 °C, suggesting the formation of radicals as in the solution state (Figure 7b). Noteworthy is that **2** showed a significantly low melting point

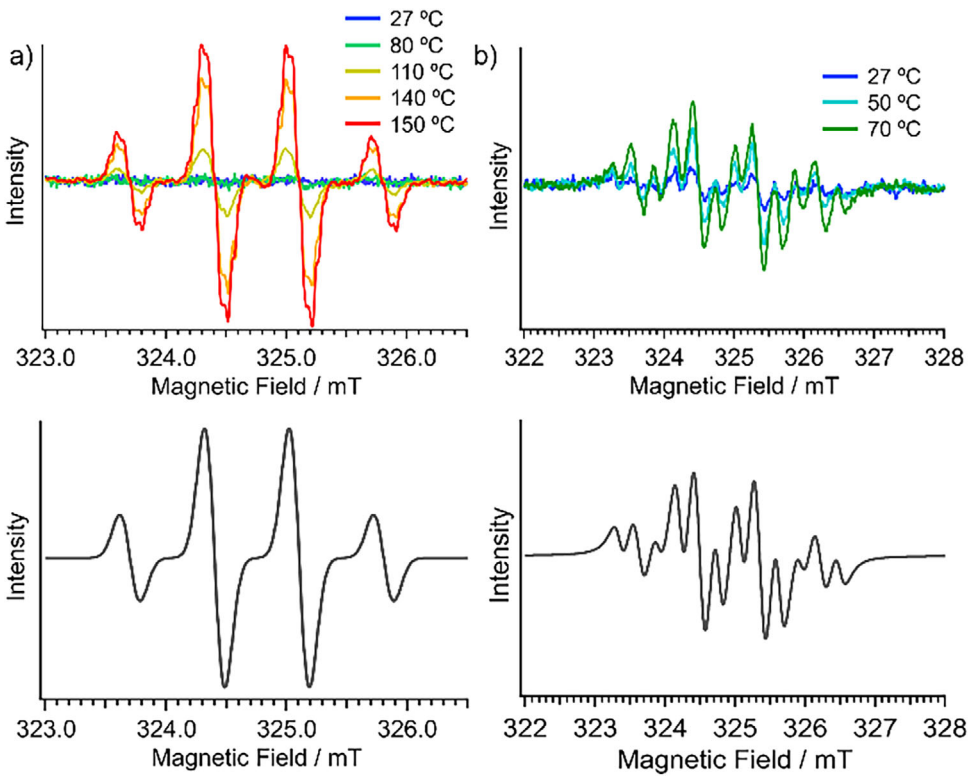

Figure 6. Temperature-dependent solution state ESR data of a) **1** and b) **2** with their simulation patterns. Sample solutions were prepared as 1.0×10^{-3} M mesitylene solution.

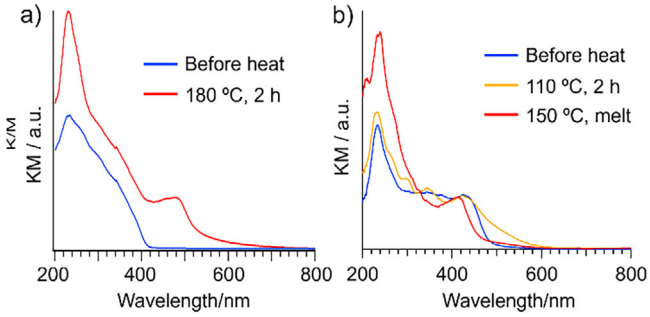

Figure 7. Diffuse reflectance spectra of solid state a) **1** and b) **2 heated at different temperatures**.

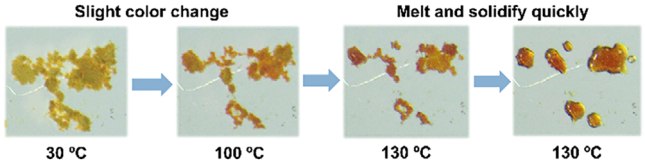

Figure 8. Phase transition process of **2** by heating on a hot glass plate.

at 130 °C compared with other reported indanedione dimers, which never showed melting before decomposition around 200 °C ~ 250 °C (Figure 8).[19,20] This phenomenon indicated the significantly weak intermolecular interaction in the solid state of **2**, which nicely supported its glass-like structure formation at low temperature instead of a single crystal. Although it is almost impossible to discuss the effect of both methylation and benzo fusion in detail due to the lack of clear solid-state structural information, this was one of the good examples of how intermolecular interactions affect the phase transition behavior. Sequential investigation of the phase transition behavior of **2** after melt confirmed the immediate formation of the glossy solid possessing a different UV absorption pattern from the initilal state, although the transformation process was too fast to trap (Figure 7b). This was probably induced by further radical reaction, which was reasonably matched with the ESR result (vide infra).

To clarify the differences observed in the solid samples of **1** and **2**, variable temperature ESR measurements were also performed on the powder samples in a degassed sealed tube. Upon heating compound **1** to 180 °C, a radical-derived signal (g = 2.0040) was clearly detected, consistent with the solid-state UV–vis absorption measurement results (Figure 9a). The temperature required for radical generation was comparable to that observed for the pyridine-incorporated derivative (**4PID**), which exhibited ESR signals at approximately 200 °C (Figure S8). Noteworthy is that the ESR signal of **1** returned to its original intensity upon cooling to room temperature, suggesting reversibility. To verify this, the heated sample was analyzed by ^{1}H NMR (Figure S9). Although small peaks, which probably formed via an unknown type of radical reaction, were observed, most of the peak retained the initial dimer pattern, and no monomeric product **1a** was detected (Figure S10). These results indicated that the reversible C—C bond scission/recombination occurred in crystalline **1**, unlike in the solution state. This behavior contrasts sharply with the irreversible bond cleavage

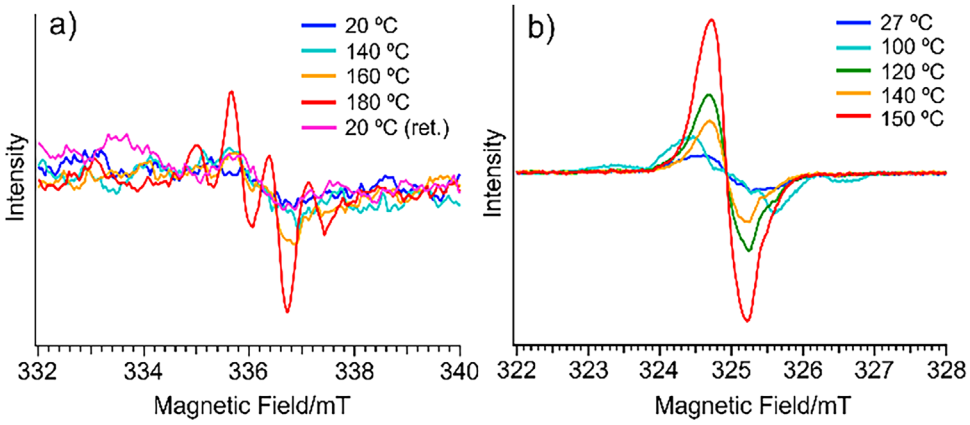

Figure 9. Temperature-dependent solid-state ESR data of a) **1** and b) **2**.

observed in solution and is likely due to the rigid, tightly packed crystalline structure. The dense packing restricts the diffusion of the generated monomer radicals, thereby relatively suppressing further reactions and enabling reversible scission and recombination of the central C—C bond.

Motivated by the above results, we carried out temperature-dependent single-crystal X-ray structure analysis of the single crystal of **1,** aiming to detect significant C—C bond elongation in the high-temperature region (Figure S11a). The central C—C bond distance of the indanedione dimer was found to be 1.564 Å at 30 °C, and only slight elongation to 1.570 Å was observed at 180 °C. This minimal change may be attributed to the limited formation of radical species, likely confined to the crystal surface, and thus not prominently reflected in the diffraction data dominated by the unreacted bulk crystal. Meanwhile, the anisotropic elongation of the lattice parameter along the *b*-axis, which is roughly parallel to the central C—C bond in the single crystal, was confirmed, suggesting that the weaker intermolecular interaction along the *b*-axis than the other two directions (Figure S11b).

In contrast, in the case of ESR pattern of **2**, a slight signal originating from radicals was observed even at room temperature, consistent with observations in the solution state (Figure 9b). Upon heating, the signal intensity gradually increased while maintaining a *g*-value of 2.0040, reaching a maximum at 120 °C, which was much lower temperature than the case of **1** (180 °C). Considering the thermal behavior and morphological changes observed in Figure 8, this lower activation temperature can be attributed to the glass-like nature of solid-state **2**, in which reduced intermolecular interactions permit greater molecular mobility and facilitate bond cleavage, unlike in the densely packed crystalline state of **1**. The signal pattern changes in this heating process also reflected the gradual morphology change around 100 °C ~ 120 °C. Further heating caused a slight decrease in signal intensity at around 140 °C, which was the temperature where the sample showed re-solidification after melting. This phenomenon likely results from partial polymerization of the monomer radicals (**2•**), forming an amorphous solid matrix in which unreacted dimers retain sufficient space to undergo further C—C bond scission, thereby regenerating **2•** upon continued heating (Figure 10). Although the signal intensity was also returned to the initial state in the case of the solid sample of **2**, the *g*-value was changed from the initial 2.0040 to 2.0036 (Figure S12). This unusual ESR pattern change was further investigated by ^{1}H-NMR measurements to find that the heated sample contained almost no dimer **2** and was mostly converted to monomer **2a** and polymer-like products with broad signals, as in the case of the solution sample. These distinct differences between the solid-state and solution behaviors of **2**, contrasting sharply with **1**, implied the crucial role of intermolecular interaction in determining thermal reactivity. Although the exact contribution of ring fusion and methyl substitution to the formation of the glass-like structure remains uncertain, the present findings clearly demonstrate their impact on solid-state dynamics.

We finally checked solid-state properties of compound **3**. However, neither diffuse reflectance spectroscopy nor ESR measurements revealed any indication of radical generation via C—C bond scission, even after heating above 150 °C. This absence of reactivity was further supported by ^{1}H NMR measurement, which showed no signs of bond cleavage or monomer formation (Figure S13). These results are consistent with the observation in solution state of **3′** and imply no contribution of its tightly packed structure to the bond scission property in the solid state.

3. Conclusion

In this study, we synthesized thiophene ring-introduced new indanedione dimers **1**, **2**, and the bridged compound **3′**, aiming to achieve low C—C bond scission temperature by means of focusing on the captodative effect for the radical stabilization as well as the steric effect caused by benzo-fuse to reduce the intermolecular interaction. In the solution state, both **1** and **2** generated corresponding radical species **1•** and **2•** upon heating, and the required temperature for the homolysis matched with the calculated BDE. Meanwhile, in the solid state, the scission temperatures were strongly affected by the strength of the intermolecular interactions. Tightly packed crystal **1** exhibited a high scission temperature of up to 180 °C, whereas **2**, which formed a glass-like, less ordered solid, generated radical species at approximately 100 °C. In contrast, the thiophene-

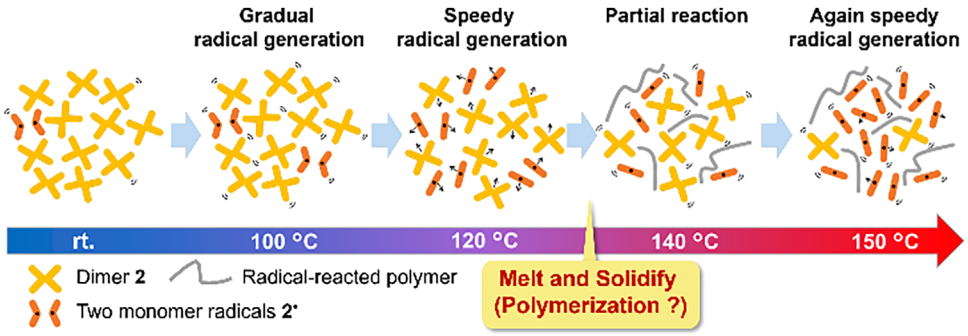

Figure 10. Schematic model of the heating effect on solid-state **2**.

bridged compound did not show significant C—C bond scission, indicating that the bridged structure suppressed the intrinsic C—C bond scission ability of indanedione dimers. These insights provide a valuable foundation for further development of stimuli-responsive magnetic and electron-conducting materials based on inclusion compounds.

4. Experimental Section

4.1. General Information

Chemical reagents and solvents were commercially purchased and purified according to the standard methods, if necessary. Air- and moisture-sensitive reactions were carried out using commercially available anhydrous solvents under an inert atmosphere of nitrogen in flame-dried glasswares. ^{1}H, ^{13}C NMR spectra were recorded on a 400 MHz JEOL JNM-ECS400 NMR spectrometer (^{1}H: 400 MHz and ^{13}C: 100 MHz). Chemical shifts (δ) are expressed relative to the resonances of the residual non-deuterated solvent for ^{1}H ($CDCl_3$: $^{1}H(\delta) = 7.26$ ppm, $(CD_3)_2SO$: $^{1}H(\delta) = 2.50$ ppm) and for ^{13}C ($CDCl_3$: $^{13}C(\delta) = 77.0$ ppm, $(CD_3)_2SO$: $^{13}C(\delta) = 39.52$ ppm). Infrared (IR) spectra were recorded on a JASCO FT/IR-4100 spectrometer using dispersed KBr pellets. Various temperature UV–vis absorption spectra were recorded on a JASCO V-670 spectrometer with a UNISOKU CoolSpek. High-temperature ESR spectra were recorded with a JEOL JES-RE1X (9.115000 GHz) X-band spectrometer, a Bruker EMX plus (9.421000 GHz), and a Bruker EMXmicro (9.575800 GHz) X-band spectrometer. Direct Analysis in Real Time (DART) Electronic Supporting Information mass spectra were measured on a JEOL JMS-T100LP spectrometer. Melting points were determined on a Stanford Research Systems Optimelt MPA100 and were uncorrected. Merck pre-coated TLC plate (silica gel 60 F_{254}) was used for thin-layer chromatography (TLC) analysis. The preparative TLC (PTLC) purification was conducted using Wakogel B-5F PTLC plates. Elemental analyses (C, H, N) were measured on a J-Science Micro corder JM10 at the Analysis Center in the University of Osaka.

4.2. General Method for the Synthesis of 2-Aryl-1,3-indanediones

To a solution of phthalide (700 mg, 5.22 mmol) in AcOEt (4.0 mL) was added aryl-carbaldehyde (5.22 mmol). Na (480 mg, 20.9 mmol) dissolved in dry MeOH (6.0 mL) was then added, followed by stirring for 18 h at 65 °C. Water was then added, and after partitioning between H_2O-AcOEt, the aqueous layer was acidified until pH 2 with 10% HCl solution to produce solid. The solid was filtered and washed with water to afford products.

2-(2,5-dimethylthiophen-3-yl)-1*H*-indene-1,3(2*H*)-dione (1a): Starting from 2,5-dimethylthiophene-3-carbaldehyde (732 mg, 5.22 mmol) giving a yellow solid (816 mg, 3.18 mmol, 61%); $R_f = 0.61$ (hexane/AcOEt = 3:2); mp: 130 °C; ^{1}H NMR (400 MHz, $CDCl_3$): δ (ppm) 8.06–8.03 (m, 2H), 7.91–7.88 (m, 2H), 6.16 (s, 1H), 4.31 (s, 1H), 2.40 (s, 3H), 2.32 (s, 3H); ^{13}C NMR (100 MHz, $CDCl_3$): δ (ppm) 198.4, 142.4, 136.6, 136.0, 135.7, 127.4, 124.5, 123.7, 54.7, 15.1, 13.5; IR (KBr, cm^{-1}): 2921, 1743, 1704, 1687, 1592, 1331, 1266, 1215, 823, 762, 621, 492; HRMS (DART): *m/z* Calcd. for $C_{15}H_{13}O_2S$ $[M + H]^+$: 257.06308. Found: 257.06204. High-quality single crystals of **1a** were prepared by the vapor diffusion method using dichloromethane and hexane as a yellow block.

2-(3-methylbenzo[*b*]thiophen-2-yl)-1*H*-indene-1,3(2*H*)-dione (2a): Starting from 3-methylbenzo[*b*]thiophen-2-carbaldehyde (920 mg, 5.22 mmol) giving an orange solid (717 mg, 2.45 mmol, 47%); $R_f = 0.41$ (AcOEt), mp: 179 °C; ^{1}H NMR (400 MHz, $CDCl_3$): δ (ppm) 8.12–8.09 (m, 2H), 7.95–7.93 (m, 2H), 7.73 (d, $J = 7.8$ Hz, 1H), 7.70 (d, $J = 7.8$ Hz, 1H), 7.40–7.36 (m, 1H), 7.33–7.29 (m, 1H), 4.76 (s, 1H), 2.41 (s, 3H); ^{13}C NMR (100 MHz, $CDCl_3$): δ (ppm) 196.8, 142.1, 140.2, 139.0, 136.4, 132.4, 127.8, 124.7, 124.3, 124.1, 122.4, 122.1, 55.0, 12.6; IR (KBr, cm^{-1}): 3056, 1664, 1615, 1595, 1558, 1524, 1436, 1302, 1274, 1174, 750, 718; HRMS (DART): *m/z* calcd. for $C_{18}H_{13}O_2S$ $[M + H]^+$: 293.06308. Found: 293.06209.

2-(benzo[*b*]thiophen-2-yl)-1*H*-indene-1,3(2*H*)-dione (3a): Starting from benzo[*b*]thiophen-2-carbaldehyde (847 mg, 5.22 mmol) giving a dark purple solid (726 mg, 2.61 mmol, 50%); $R_f = 0.52$ (MeOH/AcOEt = 1:5), mp: 215 °C; ^{1}H NMR (400 MHz, DMSO-d_6): δ (ppm) 9.00–10.00 (broad, 1H), 7.89–7.85 (m, 2H), 7.75 (d, $J = 7.6$ Hz, 1H), 7.47–7.38 (m, 4H), 7.30–7.27 (m, 1H), 7.20 (t, $J = 7.6$ Hz, 1H); ^{13}C NMR (100 MHz, DMSO-d_6): δ (ppm) 183.3, 139.6, 138.0, 136.3, 134.1, 131.8, 124.2, 123.2, 122.6, 121.9, 120.1, 118.0, 104.2; IR (KBr, cm^{-1}): 2997, 1647, 1615, 1578, 1466, 1396, 1323, 1209, 1171, 879, 859, 724; HRMS (DART): *m/z* calcd. for $C_{17}H_{11}O_2S$ $[M + H]^+$: 279.04743. Found: 279.04629.

4.3. General Method for the Synthesis of Indanedione Dimers

To a solution of 55% NaH (33.6 mg, 0.770 mmol) in dry THF (12 mL) was added 2-aryl-1,3-indandiones (0.513 mmol). After stirring for 10 min at 27 °C, $PhI(OAc)_2$ (165 mg, 0.513 mmol) was added, and the mixture was stirred for 3 h for **1** and 20 h for **2** at 27 °C. After $Na_2S_2O_3$ aq. was added, THF was evaporated. Extracted with CH_2Cl_2, the organic layer was dried over anhydrous Na_2SO_4, filtered, and concentrated under reduced pressure. After the crude mixture was purified by PTLC (hexane/THF = 2:1 for **1** and hexane/THF = 1:1 for **2**), re-precipitation with CH_2Cl_2 and hexane was performed and filtered to afford the powder samples.

2,2′-bis(2,5-dimethylthiophen-3-yl)-1*H*,1′*H*-[2,2′-biindene]-1,1′,3,3′(2*H*,2′*H*)-tetraone (1): Starting from **1a** (131 mg, 0.513 mmol)

giving a white solid (51.1 mg, 0.10 mmol, 39%); mp: 217 °C (dec.); R_f = 0.57 (hexane/AcOEt = 3:2) ^{1}H NMR (400 MHz, $CDCl_3$): δ (ppm) 7.90–7.88 (m, 4H), 7.77–7.74 (m, 4H), 6.38 (s, 2H), 2.28 (s, 6H), 2.02 (s, 6H); ^{13}C NMR (100 MHz, $CDCl_3$): δ (ppm) 197.1, 141.5, 138.1, 135.4, 133.2, 129.9, 123.8, 123.6, 65.0, 15.0, 14.8; IR (KBr, cm^{-1}): 2920, 1739, 1706, 1594, 1448, 1347, 1253, 1137, 811, 755, 665, 583; HRMS (DART): *m/z* Calcd. for $C_{30}H_{23}O_4S_2$ $[M + H]^+$: 511.10323. Found: 511.10238; E.A. Calcd. for $C_{30}H_{22}O_4S_2$: C 70.57%, H 4.34%, N 0%. Found: C 70.49%, H 4.24%, N 0%.

2,2′-bis(3-methylbenzo[*b*]thiophen-2-yl)-1*H*,1′*H*-[2,2′-biindene]-1,1′,3,3′(2*H*,2′*H*)-tetraone (2): Starting from **2a** (150 mg, 0.513 mmol) giving a yellow solid (28.4 mg, 0.049 mmol, 19%); mp: 125 °C (dec); R_f = 0.40 (hexane/AcOEt = 2:1); ^{1}H NMR (400 MHz, $CDCl_3$): δ (ppm) 7.96–7.94 (m, 4H), 7.78–7.76 (m, 4H), 7.70–7.68 (m, 2H), 7.65–7.63 (m, 2H), 7.35–7.29 (m, 4H), 2.13 (s, 6H); ^{13}C NMR (100 MHz, $CDCl_3$): δ (ppm) 194.9, 141.7, 141.3, 139.7, 135.8, 135.1, 126.4, 125.1, 124.3, 124.1, 122.5, 121.9, 65.3, 13.4; IR (KBr, cm^{-1}): 1744, 1711, 1592, 1432, 1348, 1248, 753, 728, 646, 433, 418; HRMS (DART): *m/z* calcd. for $C_{36}H_{21}O_4S_2$ $[M - H]^-$: 581.08867. Found: 581.08741.

4.4. Synthesis of Bridged Compound 3′

To a solution of 55% NaH (47.0 mg, 1.08 mmol) in dry THF (16 mL) was added **3a** (200 mg, 0.719 mmol). After stirring for 10 min at 27 °C, $PhI(OAc)_2$ (463 mg, 1.44 mmol) was added, and the mixture was stirred for 20 h at 27 °C. After $Na_2S_2O_3$ aq. was added, THF was evaporated. Extracted with CH_2Cl_2, the organic layer was dried over anhydrous Na_2SO_4, filtered, and concentrated under reduced pressure. Then the product was re-precipitated with $CHCl_3$ and hexane and filtered to obtain **3′** as an orange powder sample with poor solubility (88.6 mg, 0.16 mmol, 45%).

mp: 366 °C (dec); R_f = 0.61 (hexane/AcOEt = 1:1); ^{1}H NMR (400 MHz, $CDCl_3$): δ (ppm) 8.35 (d, J = 8.2 Hz, 2H), 7.96 (broad, 4H), 7.89 (broad, 4H), 7.80 (d, J = 8.2 Hz, 2H), 7.51–7.47 (m, 2H), 7.40–7.36 (m, 2H); IR (KBr, cm^{-1}): 1741, 1711, 1591, 1456, 1426, 1331, 1241, 1157, 1079, 1020, 994, 948, 753, 632, 616; HRMS (DART): *m/z* Calcd. for $C_{34}H_{17}O_4S_2$ $[M + H]^+$: 553.05628. Found: 553.05385. High-quality single crystals of **3′** were prepared by slow evaporation of a dichloromethane solution of **3′** as a deep orangish block.

4.5. Single Crystal X-ray Structure Analysis

The diffraction data for **1** and **3′** were recorded on a XtaLAB Synergy with a Cu-target (λ = 1.54184 Å) equipped with a Rigaku HyPix-6000HE as the detector at 123 K in-house. The high-temperature diffraction data for **1** were recorded on an ADSC Q210 CCD area detector with synchrotron radiation (λ = 0.70000 Å) as the detector at 453 K at 2D beamline in Pohang Accelerator Laboratory (PAL), Korea. The diffraction images were processed by using CrysAlisPro[31] for **1** (at 123 K) and **3′**, and HKL3000[32] for **1** (at 453 K). All the structures were solved by direct methods (SHELXT-2015, 2018/2)[33] and refined by full-matrix least squares calculations on F^2 (SHELXL-2018/3)[34] using the Olex2[35] program package.

1 (at 123 K): $C_{34}H_{16}O_4S_2$, monoclinic, space group $P2_1/n$ (No. 14), a = 10.3562(2) Å, b = 17.2125(3) Å, c = 14.2191(3) Å, β = 103.740(2)°, V = 2462.11(8) Å^3, Z = 4, ρ_{calcd} = 1.377 g cm^{-1}. 4474 unique reflections out of 4981 with $I > 2\sigma(I)$, 329 parameters, 4.104°< θ <74.255° R_1 = 0.0428, wR_2 = 0.1113, GOF = 1.068. CCDC 2429173.

1 (at 453 K): $C_{34}H_{16}O_4S_2$, monoclinic, space group $P2_1/n$ (No. 14), a = 10.3562(2) Å, b = 17.2125(3) Å, c = 14.2191(3) Å, β = 103.740(2)°, V = 2462.11(8) Å^3, Z = 4, ρ_{calcd} = 1.377 g cm^{-1}. 4474 unique reflections out of 4981 with $I > 2\sigma(I)$, 329 parameters, 4.104°< θ <74.255° R_1 = 0.0428, wR_2 = 0.1113, GOF = 1.068. CCDC 2429173.

3′: $C_{34}H_{16}O_4S_2$, orthorhombic, space group *Pbca* (No. 61), a = 17.0371(3) Å, b = 14.7959(3) Å, c = 19.6369(3) Å, $\alpha = \beta = \gamma$ = 90°, V = 4950.0(2) Å^3, Z = 8, ρ_{calcd} = 1.483 g cm^{-1}. 4107 unique reflections out of 4848 with $I > 2\sigma(I)$, 361 parameters, 4.503°< θ <75.212° R_1 = 0.0409, wR_2 = 0.1129, GOF = 1.025. CCDC 2429174.

Acknowledgments

This study was supported by a Grant-in-Aid for Scientific Research on Innovative Area 'π Space Figuration' from MEXT (No. JP26102002), Grant-in-Aid for Transformative Research Areas "Science of 2.5 Dimensional Materials" (Nos. JP21H05232 and JP21H05233), "Hyper-Ordered Structures Sciences" (Nos. JP21H05563 and JP23H04112), JSPS KAKENHI (Nos. JP24H00460, 26288020, JP15H06357, JP18K05080), JST, PRESTO (No. JPMJPR24MA) and Dynamic Alliance for Open Innovation Bridging Human, Environment and Materials (No. 20254019). This study was also conducted in Institute for Molecular Science, supported by "Advanced Research Infrastructure for Materials and Nanotechnology in Japan (ARIM)" of the Ministry of Education, Culture, Sports, Science and Technology (MEXT) (Nos. JPMXP09S20MS1046, JPMXP09S21MS1054, JPMXP1223MS1084). Y.Y. is grateful for the financial supports from the Murata Science and Education Foundation and the Iketani Science and Technology Foundation. Single-crystal X-ray diffraction studies with synchrotron radiation were performed at the High Energy Accelerator Research Organization (KEK) (2022G131) and the Pohang Accelerator Laboratory (2023-2nd-2D-042). The theoretical calculations were performed at the Research Centre for Computational Science, Okazaki, Japan (25-IMS-C060). We thank Dr. Yuta Uetake for the fruitful discussion about the racemization energy evaluation of **3′**, and Dr. Takuya Kodama for the suggestive comments for ESR peak assignment.

Conflict of Interests

The authors declare no conflict of interest.

Keywords: Captodative effect · Dynamic covalent bond · Indanedione dimers · Phase transitions · Radicals

[1] B. L. Feringa, R. A. van Delden, N. Koumura, E. M. Geertsema, *Chem. Rev.* **2000**, *100*, 1789–1816.
[2] V. Balzani, A. Credi, F. M. Raymo, J. F. Stoddart, *Angew. Chem., Int. Ed.* **2000**, *39*, 3348-3391.
[3] D. Qu, Q. Eang, Q. Zhang, X. Ma, H. Tian, *Chem. Rev.* **2015**, *115*, 7543-7588.
[4] D. Roy, W. L. A. Brooks, B. S. Sumerlin, *Chem. Soc. Rev.* **2013**, *42*, 7214.
[5] Z. Liu, W. Qi, G. Hu, *Chem. Soc. Rev.* **2015**, *44*, 3117-3142.
[6] P. Xue, J. Ding, P. Wang, R. Lu, *J. Mater. Chem. C* **2016**, *4*, 6688-6706.
[7] T. Seki, H. Ito, *Chem. - Eur. J.* **2016**, *22*, 4322-4329.
[8] S. J. Rowan, S. J. Cantrill, G. R. L. Cousins, J. K. M. Sanders, J. F. Stoddart, *Angew. Chem. Int, Ed.* **2002**, *41*, 898-952.
[9] Y. Jin, C. Yu, R. J. Denman, W. Zhang, *Chem. Soc. Rev.* **2013**, *42*, 6634.
[10] D. Sakamaki, S. Ghosh, S. Seki, *Mater. Chem. Front.* **2019**, *3*, 2270-2282.
[11] Y. Kobayashi, J. Abe, *Chem. Soc. Rev.* **2022**, *51*, 2397-2415.
[12] T. Yamamoto, A. Takahashi, H. Otsuka, *Bull. Chem. Soc. Jpn.* **2024**, *97*, uoad004.

[13] D. Harnack, W. Krull, M. Lehnig, W. P. Neumann, A. K. Zarkadis, *J. Chem. Soc. Perkin Trans. 2* **1994**, 1247.
[14] I. V. Khudyakov, Y. I. Kiryukhin, A. I. Yasmenko, *Chem. Phys. Lett.* **1980**, *74*, 462-466.
[15] L. M. Pisarenko, A. B. Gagarina, V. A. Roginskii, *Izv. Akad. Nauk SSSR, Ser. Khim.* **1987**, *12*, 2861.
[16] Z. G. Aliev, A. N. Chekhlov, L. O. Atovmyan, L. M. Pisarenko, V. I. Nikulin, *Zh. Strukt. Khim.* **1990**, *31*, 103.
[17] A. A. Dadari, I. P. Lastenko, *J. Solid State Chem.* **1992**, *98*, 330.
[18] A. A. Dadari, I. P. Lastenko, M. A. Kojushner, *J. Solid State Chem.* **1993**, *102*, 289.
[19] Y. Yakiyama, T. Fujinaka, M. Nishimura, R. Seki, H. Sakurai, *Chem.Commun.* **2020**, *56*, 9687-9690.
[20] Y. Yakiyama, T. Fujinaka, M. Nishimura, R. Seki, H. Sakurai, *Asian J. Org. Chem.* **2021**, *10*, 2690-2696.
[21] S. Park, J. Lee, H. Jeong, S. Bae, J. Kang, D. Moon, J. Park, *Chem* **2022**, *8*, 1993-2010.
[22] S. Park, J. Lee, B. Kim, C. Jung, S. Bae, J. Kang, D. Moon, J. Park, *J. Am. Chem. Soc.* **2024**, *146*, 9293-9301.
[23] H. G. Viehe, Z. Janousek, R. Merenyi, L. Stella, *Acc. Chem. Res.* **1985**, *18*, 148-154.
[24] F. G. Bordwell, T.-Y. Lynch, *J. Am. Chem. Soc.* **1989**, *111*, 7558-7562.
[25] T. Yasui, T. Kikuchi, Y. Yamamoto, *Chem. Commun.* **2020**, *56*, 12865-12868.
[26] K. Matsuo, R. Okumura, H. Hayashi, N. Aratani, S. Jinnai, Y. Ie, A. Saeki, H. Yamada, *Chem. Commun.* **2022**, *58*, 13576-13579.
[27] J. Grover, M. Raghu, R. Hazra, S. S. V. Ramasastry, A. Mondal, *Synthesis* **2018**, *50*, 1462.
[28] J. G. Lombardino, E. H. Wiseman, *J. Med. Chem.* **1968**, *11*, 342-347.
[29] J. A. Baird, B. V. Eerdenbrugh, L. S. Taylor, *J. Pharm. Sci.* **2010**, *99*, 3787-3806.
[30] M. Y. Lo, C. Zhen, M. Lauters, G. E. Jabbour, A. Sellinger, *J. Am. Chem. Soc.* **2007**, *129*, 5808-5809.
[31] CrysAlisPRO, Rigaku Oxford Diffraction, Yarnton, England **2015**.
[32] W. Minor, M. Cymborowski, Z. Otwinowski, M. Chruszcz, *Acta Crystallogr., Sect. D: Biol. Crystallogr.* **2006**, *62*, 859-866.
[33] G. M. Sheldrick, *Acta Crystallogr., Sect. A: Found. Adv.* **2015**, *71*, 3-8.
[34] G. M. Sheldrick, *Acta Crystallogr., Sect. C: Struct. Chem.* **2015**, *71*, 3-8.
[35] O. V. Dolomanov, L. J. Bourhis, R. J. Gildea, J. A. K. Howard, H. Puschmann, *J. Appl. Crystallogr.* **2009**, *42*, 339-341.

Manuscript received: May 9, 2025
Revised manuscript received: July 5, 2025
Version of record online: ■■, ■■